Numerical investigation of heat transfer enhancement in a pipe partially filled with a porous material under local thermal non-equilibrium condition

Y. Mahmoudi[1,*], N. Karimi[2]

[1] *Department Process and Energy, Delft University of Technology, Delft, The Netherlands*

[2] *Department of Engineering, University of Cambridge, Cambridge, United Kingdom*

* *Corresponding author: Tel.: +31-152786745; email: s.y.mahmoudilarimi@tudelft.nl*

Abstract

This paper examines numerically the heat transfer enhancement in a pipe partially filled with a porous medium under Local Thermal Non-Equilibrium (LTNE) condition. The flow inside the porous material is modelled using the Darcy-Brinkman-Forchheimer model. The effect of different parameters such as, inertia (F), Darcy number (Da), conductivity ratio, porosity and particle diameter on the validity of Local Thermal Equilibrium (LTE) are studied. The optimum porous thickness for heat transfer enhancement under varying F and with reasonable pressure drop is determined. The pipe wall is under constant wall temperature boundary condition. Two models are considered at the interface between the porous medium and the fluid. The differences between these models in predicting the temperature of the fluid and solid phases as well as the Nusselt (Nu) number for different pertinent parameters are discussed. In general, the two interface models result in similar trends of Nu number variation versus porous thickness ratio. However, considerably different values of Nu number are obtained from the two interface models. The effects of inertia term on the Nu number and pressure drop are further studied. For a given model and for Da<10^{-3}, the Nu number is found independent of F. However, for Da>10^{-3} as F increases the computed Nu number increases.

Key words: Heat transfer enhancement, porous media, inertia term, porous-fluid interface, local thermal non-equilibrium.

---

1. Introduction

Fluid flow and forced convection heat transfer in porous media are of high academic and industrial significance [1]. These problems have a wide range of applications in natural and manmade systems. These include heat exchangers, cooling of electronic components, biological systems, geothermal engineering, solid matrix heat exchangers, enhanced oil recovery, thermal insulation, chemical reactors and other areas [1]. In some applications there is no need to completely fill the system with the porous material and a partial filling is sufficient. Partial filling has the important advantage of reducing the pressure drop in comparison to a system filled completely with porous medium [2, 3]. The general problem of forced convection in partially filled pipes and channels has received a decent attention in the literature. Poulikakos and Kazmierczak [4] analytically solved the problem of forced convection in channels partially filled with porous materials. They reported that there is an optimum value of porous thickness at which the Nusselt number reaches its minimum value [4]. Numerical studies of force convection in a pipe with a porous material inserted at the core of the pipe revealed that significant heat transfer enhancement can be achieved at the expense of a reasonable pressure drop [2, 5, 6]. The influences of porous insert configuration upon heat transfer have been further studied in a numerical investigation by Maerefat et al. [3]. It was shown that if the porous material is inserted at the core of the pipe, the heat transfer rate increases. However, when the porous material is attached to the internal wall of the pipe the Nusselt number is lower than that of a pipe without porous insert [3]. Study of forced convection in a partially filled channel under Local Thermal Equilibrium (LTE) revealed that the maximum value of Nusselt number occurs at the porous thickness to pipe radius ratio of 0.8 and Darcy number of 10^{-3} [7]. It has been, further, shown that enhancement of heat transfer by porous material depends on the ratio of the effective thermal conductivity of the porous medium to that of the fluid [8]. Bhargavi et al. [9] studied the effects of porous material on heat transfer rate in a channel partially filled with porous materials under LTE condition. Their results showed that the change in the Nusselt numbers at the two walls was negative for small porous thickness. Numerical investigation of turbulent flow in a pipe partially filled with a porous material showed that for enhancement of heat transfer the optimum ratio of porous medium thickness to pipe diameter is 0.8 [10]. Ucar et al. [11] and Cekmer et al. [12] studied numerically and analytically the steady, laminar, and fully developed forced convection heat transfer in a parallel plate channel through LTE model under constant heat flux boundary conditions. A comprehensive review of the investigations on forced convection in partially filled porous channel can be found in the work of Ucar et al. [11]. They covered different aspects of the problem concerning dimensions, governing equations, outer surface thermal conditions and solution methods. In the work of Cekmer et al. [12] the Nusselt number and pressure drop increment ratios were used to define a performance of the porous-channel system. They argued that for a partially porous filled channel, the performance is highly influenced by Darcy number.

Most of the references cited so far assumed LTE condition in their analyses. There are, in general, two different approaches to thermal energy transport in porous media. These include Local Thermal Equilibrium (LTE) and Local Thermal Non-Equilibrium (LTNE). The LTE model assumes that locally the solid phase temperature is equal to that of the fluid phase. This immediately defines the thermal boundary conditions between the two phases and eliminates the burden of finding and implementing them. It therefore significantly facilitates the heat transfer analysis. The LTNE model, however, requires additional information to account for the modes of energy communication between the two considered phases. The thermal boundary conditions should now be specified on the porous-fluid interface [13]. Different boundary conditions and the physics of the porous-fluid interface have been subjected to some investigations (e.g. [14] and [15]). Jamet and Chandesris [14] studied the physical nature of different parameters involved in the jump conditions at the interface of a porous-clear region. d'Hueppe et al. [15] studied the jump relations at the porous-clear region under the assumption of local thermal equilibrium condition. The interface models have been further included into LTNE analyses. Vafai and Thiyagaraja [16] analytically investigated the velocity and temperature fields at the interface region. They used the Brinkman-Forchheimer extended Darcy equation and considered three fundamental types of interface. These included the interfaces between two porous regions, a porous medium and a fluid layer and a porous medium and an impermeable medium. An exact solution for the fluid mechanics of the interface region between a porous medium and a fluid layer was put forward by Vafai and Kim [17]. This solution accounts for both boundary and inertial effects.

Upon application of a heat flux to the outer surface of a porous medium, the applied heat is transferred to the solid and fluid parts. Amiri et al. [18] argued that the constant heat flux boundary condition could be viewed in two different ways. The first is to assume that heat division between the two phases is on the basis of their effective conductivities and the corresponding temperature gradients. The second approach is to assume that each of the individual phases at the interface receives an equal amount of the prescribed heat flux. In the study of Amiri et al. [18] good agreements were observed between the numerical results based on the second approach and the experimental data. Lee and Vafai [19] and Marafai and Vafai [20] used the first approach to obtain analytical solutions for the temperature profiles, the temperature difference between the two phases and the Nusselt number. Yang and Vafai [13] studied analytically the fully developed flow in a channel partially filled with a porous medium. These authors considered five forms of thermal conditions at the interface between a porous medium and a fluid under LTNE and proposed exact solutions for all of these conditions. They further reported the restrictions on the validity of LTE in a channel partially filled with a porous material. Yang et al. [21] studied analytically the validity of LTE for the case of thermally fully developed flow in a tube filled with a porous medium under constant wall heat flux. They found that the local thermal equilibrium assumption may fail for the case of constant heat flux wall. Validity of LTE in a pipe partially filled with a porous material has been investigated under two different configurations [22]. It was found that LTE is not valid when the porous material is attached to the pipe wall. A comprehensive study was conducted by Alazmi and Vafai [23] who analysed the effect of different boundary conditions, under constant wall heat flux and LTNE condition. They studied six models based on the first approach and two models based on the second approach of Amiri et al. [18]. It was reported that depending on the application area either of the two models can be a representative boundary condition. Alazmi and Vafai [23] referred to the model based on the first approach as model A and that based on the second approach as model B. In keeping with these authors, the same terminology is used in this paper. Most recently Vafai and Yang [24] argued that heat flux bifurcations at the porous-clear region interface is such a fundamental issue that can open a new research direction. In a separate work Yang and Vafai [25] investigated heat flux bifurcation inside a porous medium in a channel partially filled with a porous material under LTNE condition. The effects of thermal dispersion and inertia were taken into account in their study. They subsequently determined the validity range of LTE condition. Previous studies on pipes partially filled with porous material under LTE, have shown that for Darcy numbers less than 10^{-3} the effect of inertia term on Nusselt number is negligible [2, 3, 26]. However, at high Darcy numbers the thermal field depends on the inertia term. These studies then considered only small Darcy numbers and omitted the inertia term in their simulations. No study, so far, has considered a pipe partially filled with porous material with high Darcy number to investigate the effect of inertia parameter on heat transfer enhancement. This lack of study extends to both LTE and LTNE models. Neither has been any investigation on the influence of interface models and pertinent parameters such as porosity, particle diameter and Forchheimer parameter upon the validity of LTE condition.

The present work aims at filling these gaps through a series of numerical investigations. The problem includes forced convection flow in a pipe partially filled with a porous medium under LTNE condition. The pipe wall is subjected to the constant wall temperature. The Darcy-Brinkman-Forchheimer model is used for the flow transport while two-equation model is employed for energy transport in the porous medium. Two models are considered at the interface between the porous medium and the clear region to represent the flux bifurcation. The effects of porous thickness ratio and different pertinent parameters on the validity of LTE and Nusselt number are then analysed. These include Darcy number, inertia parameter, porosity, particle diameter and solid-to-fluid conductivity ratio. The main emphasis of the present work is on:

i. determination of porous material thickness up to which the local thermal equilibrium between the solid phase and fluid phase is valid as a function of different pertinent parameters ($R_{r,\,LTE}$),

ii. the influences of different models utilised at the interface of porous-fluid on the validity of LTE,

iii. the effects of different parameters such as, Forchheimer term, Darcy number, conductivity ratio, porosity and particle diameter on the validity of LTE,

iv. determination of porous thickness which maximises the Nusselt number for the two porous-fluid interface models ($R_{r,\,Nu}$),

v. the effect of pertinent parameters including Darcy number, porous thickness and inertia parameter on the disparities between the results obtained through various porous-fluid interfaces,

vi. the role of inertia parameter in determining the optimum porous thickness for heat transfer enhancement by considering a reasonable pressure drop.

The range of validity of LTE is determined for two fundamental models in terms of different physical parameters. This is of crucial importance since the inappropriate use of the interface conditions can result in significant errors in Nusselt number calculations [13].

2. Configuration of the problem

Figure 1 schematically shows the problem under investigation. Porous material is placed along the centreline of a tube filling it either partially or completely. The fluid flow enters the tube with constant and uniform velocity and temperature. The wall temperature is constant and higher than the fluid temperature at the inlet.

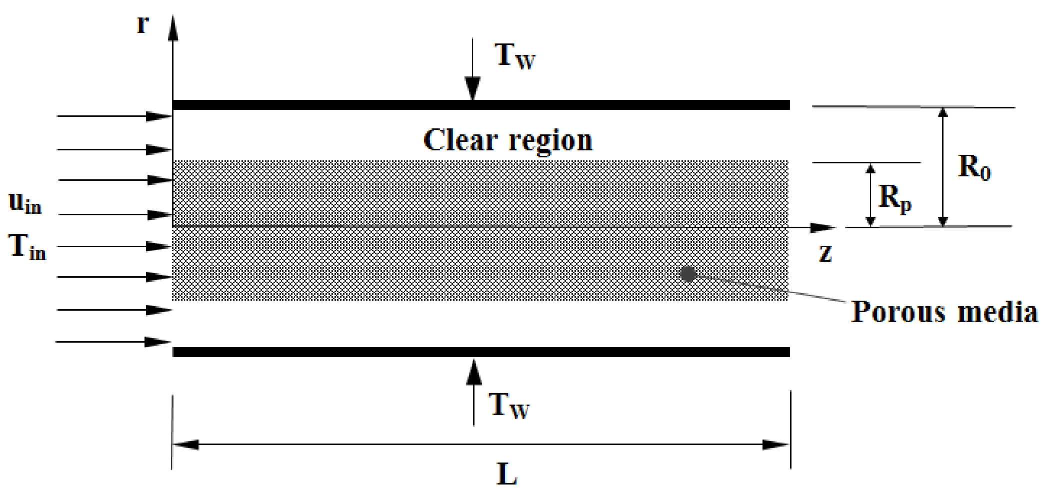

Fig.1. Schematic of the problem.

The radius of the porous material is R_p and that of the tube is R_0. The fluid moves along the *z*-axis which is co-incident with the tube centreline and perpendicular to *r*- axis. Fluid enters the tube at the inlet temperature of 300 K (i.e. T_{in} = 300 K). The tube wall temperature is kept constant at T_w = 1000 K. The thermo-physical properties of the investigated fluid and solid phases are listed in table 1. The simulations were performed for air and porous material of AISI 304. These were repeated for water and porous media of soda lime material to evaluate the influence of various thermal conductivity ratios.

Fluid phase

Viscosity $\mu\times10^5$ (kg.m^{-1}.s^{-1})	Conductivity $k_f\times10^3$ (W.m^{-1}.K^{-1})	Specific heat C_p (J.kg^{-1}.K^{-1})	Density ρ_f (kg.m^{-3})	fluid
1.9	28	1008	1.1	air
57.7	640	4180	989	water

Solid phase

Conductivity k_s (W.m^{-1}.K^{-1})	Specific heat capacity C_p (J.kg^{-1}.K^{-1})	Density ρ_s (kg.m^{-3})	Solid
15.2	485	7900	AISI304
1.4	835	2225	Soda lime

Table 1: Thermo-physical properties of the investigated fluids and solids

3. Governing equations and boundary conditions

A steady, two dimensional, laminar and incompressible flow is considered here. The viscous heat generation is ignored and there is no internal heat production. Radiation and natural convection are further ignored and the thermodynamic properties are assumed constant. Local thermal non-equilibrium condition between the solid and fluid is assumed through using two-energy equation. Under these conditions the governing equations are expressed in cylindrical coordinate [2, 3, 27]. This yields,

continuity

$$\frac{\partial}{\partial z}(\rho u)+\frac{1}{r}\frac{\partial}{\partial r}(r\rho v)=0\,, \tag{1}$$

momentum in *z*- direction in the clear region ($R_p<r<R_0$)

$$\frac{\partial}{\partial z}(\rho uu)+\frac{1}{r}\frac{\partial}{\partial r}(r\rho vu)=-\frac{\partial P}{\partial z}+\frac{\partial}{\partial z}(\mu_f\frac{\partial u}{\partial z})+\frac{1}{r}\frac{\partial}{\partial r}(r\mu_f\frac{\partial u}{\partial r}), \tag{2}$$

momentum in *r*- direction in the clear region ($R_p<r<R_0$)

$$\frac{\partial}{\partial r}(\rho uv)+\frac{1}{r}\frac{\partial}{\partial r}(r\rho vv)=-\frac{\partial P}{\partial r}+\frac{\partial}{\partial z}(\mu_f\frac{\partial v}{\partial z})+\frac{1}{r}\frac{\partial}{\partial r}(r\mu_f\frac{\partial v}{\partial r})-\frac{\mu_f v}{r^2}, \tag{3}$$

energy equation for the fluid in the clear region ($R_p<r<R_0$)

$$\frac{\partial}{\partial z}(\rho_f c_p u T_f)+\frac{1}{r}\frac{\partial}{\partial r}(\rho_f c_p r v T_f)=\frac{\partial}{\partial z}(k_f\frac{\partial T_f}{\partial z})+\frac{1}{r}\frac{\partial}{\partial r}(r k_f\frac{\partial T_f}{\partial r}), \tag{4}$$

momentum in z- direction in the porous region ($0<r<R_p$)

$$\begin{aligned}&\frac{\partial}{\partial z}(\frac{\rho}{\varepsilon}uu)+\frac{1}{r}\frac{\partial}{\partial r}(r\frac{\rho}{\varepsilon}vu)=-\frac{\partial P}{\partial z}+\frac{\partial}{\partial z}(\frac{\mu_f}{\varepsilon}\frac{\partial u}{\partial z})+\\&\frac{1}{r}\frac{\partial}{\partial r}(r\frac{\mu_f}{\varepsilon}\frac{\partial u}{\partial r})-\frac{\mu_f u}{K}-\frac{\rho F\varepsilon}{\sqrt{K}}|u|u,\end{aligned} \tag{5}$$

momentum in r- direction in the porous region ($0<r<R_p$)

$$\begin{aligned}&\frac{\partial}{\partial r}(\frac{\rho}{\varepsilon}uv)+\frac{1}{r}\frac{\partial}{\partial r}(r\frac{\rho}{\varepsilon}vv)=-\frac{\partial P}{\partial r}+\frac{\partial}{\partial z}(\frac{\mu_f}{\varepsilon}\frac{\partial v}{\partial z})+\\&\frac{1}{r}\frac{\partial}{\partial r}(r\frac{\mu_f}{\varepsilon}\frac{\partial v}{\partial r})-\frac{\mu_f v}{K}-\frac{\rho F\varepsilon}{\sqrt{K}}|u|v-\frac{\mu_f v}{\varepsilon r^2},\end{aligned} \tag{6}$$

energy equation for the fluid phase in the porous region ($0<r<R_p$)

$$\begin{aligned}&\frac{\partial}{\partial z}(\rho_f c_p u T_f)+\frac{1}{r}\frac{\partial}{\partial r}(\rho_f c_p r v T_f)=\frac{\partial}{\partial z}(k_{fe}\frac{\partial T_f}{\partial z})+\\&\frac{1}{r}\frac{\partial}{\partial r}(r k_{fe}\frac{\partial T_f}{\partial r})+h_{sf}a_{sf}(T_s-T_f),\end{aligned} \tag{7}$$

energy equation for the solid phase in the porous region ($0<r<R_p$)

$$0=\frac{\partial}{\partial z}(k_{se}\frac{\partial T_s}{\partial z})+\frac{1}{r}\frac{\partial}{\partial r}(r k_{se}\frac{\partial T_s}{\partial r})-h_{sf}a_{sf}(T_s-T_f). \tag{8}$$

In the above equations u is the so-called superficial velocity and p is the intrinsic macroscopic pressure. Indices f and s respectively denote fluid and solid. μ, ρ and C_p are respectively viscosity, density and specific heat capacity of the fluid. K is the permeability and ε is the porosity of the porous media. The effective conductivities of the porous media and the fluid are respectively k_{se} and k_{fe}. These two are geometrical functions of the porous media and conductivity of solid (k_s) and fluid (k_f) and are expressed as follows,

$$\begin{aligned}&k_{se}=(1-\varepsilon)k_s,\\&k_{fe}=\varepsilon k_f.\end{aligned} \tag{9}$$

Permeability of the porous media and the geometrical function can be written as [23]

$$K=\frac{\varepsilon^3 d_p^2}{150(1-\varepsilon)^2}, \tag{10}$$

$$F = \frac{1.75}{\sqrt{150\varepsilon^{3/2}}}, \tag{11}$$

where d_p is the diameter of the particles. Specific surface area appearing in the energy equations is expressed as

$$a_{sf} = \frac{6(1-\varepsilon)}{d_P}, \tag{12}$$

The following correlation is used for the fluid-to-solid heat transfer coefficient [23],

$$h_{sf} = k_f \left[2 + 1.1\mathrm{P_r Re_p}^{0.6}\right] / d_p . \tag{13}$$

Due to the symmetry of the problem only the upper half of the tube is considered. At $r = 0$ symmetry causes the gradients of the axial velocity and temperature in r direction to be zero. At the entrance, $z = 0$, $v = 0$, $T = T_{in}$ and $u = u_{in}$ while at the exit, $z = L$, the gradients of v, u and T in z direction are zero. In summary, the boundary conditions are [2, 3]:

$$\begin{cases} \dfrac{\partial u}{\partial r} = 0 \\ v = 0 \\ \dfrac{\partial T}{\partial r} = 0 \end{cases} \quad \text{at } r = 0$$

$$\begin{cases} u = 0 \\ v = 0 \\ T = T_w \end{cases} \quad \text{at } r = R_0$$

$$\begin{cases} u = u_{in} \\ v = 0 \\ T = T_{in} \end{cases} \quad \text{at } z = 0 \tag{14}$$

$$\begin{cases} \dfrac{\partial u}{\partial z} = 0 \\ \dfrac{\partial v}{\partial z} = 0 \\ \dfrac{\partial T}{\partial z} = 0 \end{cases} \quad \text{at } z = L$$

The following models are used to match the conditions for heat transfer at the boundary between the porous medium and the fluid [13, 25, 28].

Model A:

$$-k_{se}\left.\frac{\partial T_s}{\partial r}\right|_{R_p^-} - k_{fe}\left.\frac{\partial T_f}{\partial r}\right|_{R_p^-} = -k_f\left.\frac{\partial T_f}{\partial r}\right|_{R_p^+} = q_{\text{interface}},$$

$$T_s\big|_{R_p^-} = T_f\big|_{R_p^-},$$

and model B:

$$-k_{se}\left.\frac{\partial T_s}{\partial r}\right|_{R_p^-} = -k_f\left.\frac{\partial T_f}{\partial r}\right|_{R_p^+} = q_{\text{interface}},$$

$$-k_{fe}\left.\frac{\partial T_f}{\partial r}\right|_{R_p^-} = -k_f\left.\frac{\partial T_f}{\partial r}\right|_{R_p^+} = q_{\text{interface}}, \tag{15}$$

where $q_{\text{interface}}$ is the heat flux at the interface, which represents the thermal energy transferred through the porous region.

These two models state the continuity of heat flux at the interface of the porous region and the external fluid. In model A the heat flux, transferred from the external fluid to the porous media is distributed unevenly between the two phases. This distribution is based upon the effective conductivity of the two phases and their temperature gradient on the interface. However, in model B, each phase (solid and fluid) separately receives equal heat flux from the external fluid.

Vafai and Kim [8] presented an exact solution for the fluid flow at the interface between a porous medium and a fluid layer. Their solution included inertia and boundary effects. In this study, the shear stress in the fluid and the porous medium were taken to be equal at the interface region. In the work of Vafai and Thiyagaraja [16] continuity of shear stress and heat flux were taken into account while employing the Forchheimer-Extended Darcy equation. The current work employs one of the models used in the Refs. [16, 29]. The following momentum boundary conditions apply at the interface between the solid phase and the external fluid [3, 26, 29, 30],

$$u\big|_{R_p^-} = u\big|_{R_p^+},$$

$$\mu_e\left.\frac{\partial u}{\partial r}\right|_{R_p^-} = \mu_f\left.\frac{\partial u}{\partial r}\right|_{R_p^+}. \tag{16}$$

In Eq. (16) the shear stress and the velocity in the fluid and the porous medium were taken to be equal at the interface region [29]. In the above equation μ_e is an effective viscosity of the porous medium. It is an artificial quantity associated with the Brinkman term in the momentum equation. Alazmi and Vafai [29] showed that significant changes of the effective viscosity (from μ_f to $7.5\mu_f$) have a minor effect on the velocity distribution. It was also found that changing the effective viscosity, even within such a wide range, has no effect on the temperature and Nusselt number [29]. Therefore, in the current study μ_e is set equal to μ_f . In fact, $\mu_e = \mu_f$ is a good approximation in the range of 0.7 < ε <1 and has been widely used in the literature [2, 3, 5, 25, 26, 28].

Model A, model B and relation (16) express the continuity of heat and stress fluxes, and velocity on the interface between the solid phase and the external fluid. Relation (16) equates the shear stress in the porous media with that in the external fluid.

The local Nusselt (Nu) number for constant wall temperature is defined as follows [23, 26, 31]

$$\mathrm{Nu} = -\frac{2R_0}{T_w - T_m}\left(\frac{\partial T}{\partial r}\right)_{r=R_0}, \tag{17}$$

where the mean temperature is defined by

$$T_m = \frac{1}{U_m R_0^{\,2}} \int_0^{R_0} uTr\,dr, \tag{18}$$

and the mean velocity is

$$U_m = \frac{1}{R_0^{\,2}} \int_0^{R_0} ur\,dr. \tag{19}$$

4. Numerical method

To solve the conservation equations a controlled volume, finite-volume approach is utilised. The SIMPLE algorithm [32] was adopted to solve the flow field. The upwind first-order scheme was used to discretise the convective term and second order central difference scheme was used to discretise the diffusive term. To avoid checkerboard pressure oscillations, cell face pressure has been calculated using linear interpolation, which has the same accuracy as the central difference approximation. The algebraic equations were solved using a line-by-line technique. For the momentum and energy equations, the velocity components were under-relaxed by a factor of 0.8. For most calculations 5000 iterations were sufficient to obtain a convergent solution in a 100 × 60 grid. A non-uniform grid with a large concentration of nodes close to the boundaries was employed. Figure 2 depicts the computational domain. In comparison to z- direction, finer grids have been used in r- direction. Very fine grids were used at the inlet of the pipe to capture properly the transient region of the pipe.

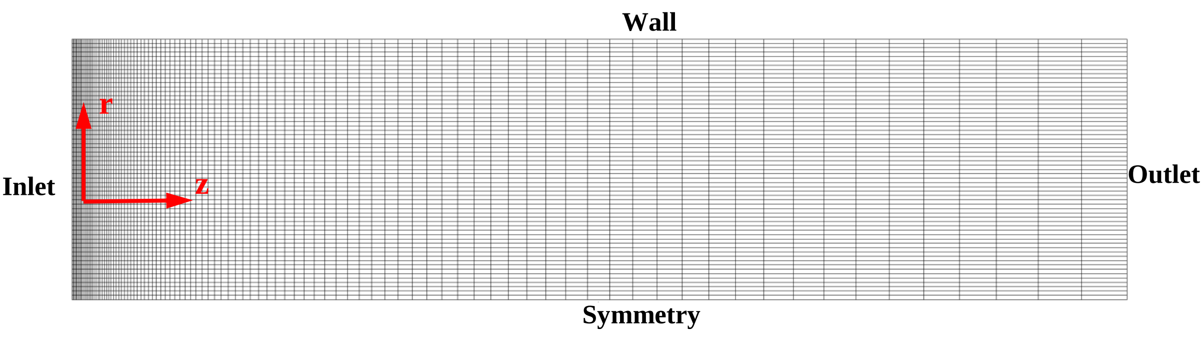

Fig. 2. The computational domain of 100 × 60 grid.

In the current study the tube length for air flow is considered 1.0 m. This increases to 2.0 m for water flow and in either case the pipe diameter is 0.2 m. These pipe dimensions are much longer than the temperature and velocity developing lengths which are of the order of $X_{hdrodynamic} \cong 0.04D\mathrm{Re}_D$ and $X_{thermal} \cong 0.04D\mathrm{Re}_D P_r$, respectively [31]. Furthermore adding porous media partially into the pipe can reduce the developing length by 50% or more [2]. To ensure the independency of the Nusselt number upon the grid resolution, a typical case with $\mathrm{R_r} = 0.8$, Da = 10^{-3}, $F = 0$, Re = 60 and based on model B was calculated. Different size meshes, 30×15, 50×30, 80×40, 100×60 and 120×80 in z- and r-directions, respectively, were employed to test the numerical model. Figure 3 shows that increasing the grid points, results in the convergence of the computed Nusselt number. The results obtained for 100×60 and 120×80 are very much the same. Hence, the grid size of 100×60, in z- and r- directions, respectively, was used for all the computations in the present work. The convergence criterion was max $(|T_{new} - T_{old}|) < 10^{-8}$, where $T_{new} - T_{old}$ is the temperature difference between two successive iterations.

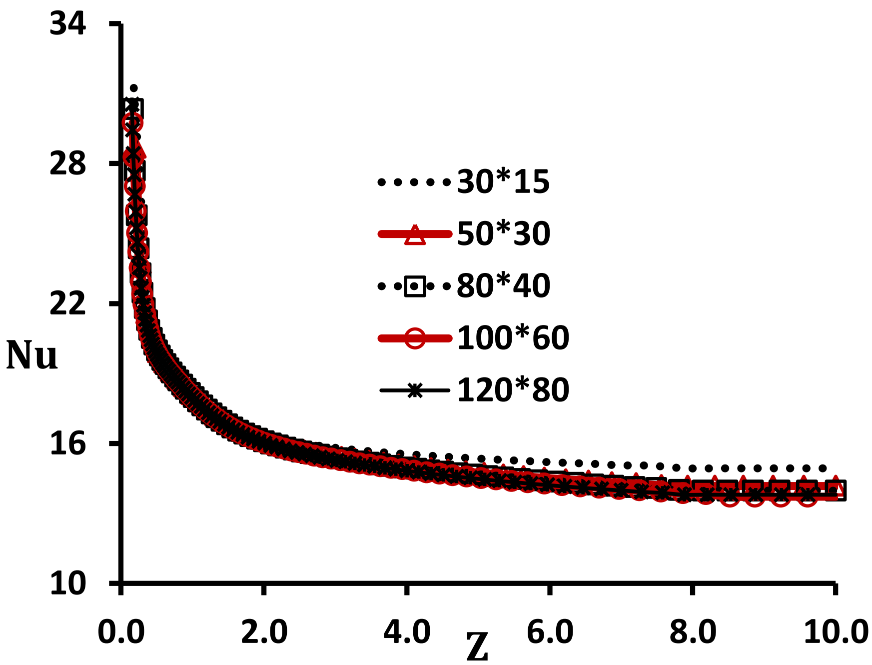

Fig. 3. Grid independency of Nusselt number versus dimensionless axial coordinate for $\mathrm{R_r} = 0.8$, Da = 10^{-3}, $F = 0$ and model B.

The LTE version of the current code has been successfully used to study heat transfer and fluid flow in porous media containing pipes and channels under laminar and turbulent regimes [3, 33].

5. Results and discussion

In the first part of this section model B is used to calculate an optimum thickness of the porous material. This is the maximum radius of the porous material which allows local thermal equilibrium ($R_{r,\ LTE}$). A parametric study is conducted. The varying parameters are Darcy number, inertia parameter, conductivity ratio, porosity and porous diameter. The effect of utilising different boundary conditions at the interface (i.e. models A and B) are then investigated. A non-dimensional temperature is defined as $\Theta = \dfrac{T_w - T}{T_w - T_{in}}$ where T_w is the wall temperature and T_{in} is the fluid temperature at the inlet. Amiri and Vafai [34] examined the LTE condition by comparing the temperature distributions of the fluid and solid phases locally. They reported that the LTE assumption holds if $|\Theta_s\text{-}\Theta_f|\times 100$ is between 1% and 5%. Thus, in the current study the criterion for local thermal equilibrium condition is $|\Theta_s\text{-}\Theta_f|\times 100 < 3\%$ [34]. Using this criterion LTE holds when the difference between the dimensional temperatures of the fluid and solid phases is less than 0.2 K. Further, it was observed that the results are independent of the inlet temperature and the tube wall temperature.

For validation purposes, the computed Nu number, based on the LTE model, is compared to the analytical solution of Kaviany [35]. This solution considers fully developed Nusselt number for laminar flow through a fully filled (R_r = 1) porous channel bounded by isothermal plates with no Forchheimer term. Figure 4 depicts a good agreement between the numerical results and the analytical solution. Further, the analytical solution predicts the fully developed Nusselt number in a pipe without porous material to be 3.660 [35]. The present simulation with Da = 10 finds this value as 3.648. The excellent agreement between these two values is another validation for the numerical simulation.

In addition, the computation was performed for d_p=0.016 m, ε=0.9, k_s/k_f=542, F=0, Da=10^{-6}, R_r=0.8 and model A. Under such parameters the temperature of the fluid and solid phases are the same. Therefore, Nusselt number was found to be Nu=22.35, which is very close to the Nusselt number for a pipe under LTE model, Nu=22.65 [2, 3]. Further, for the fully filled pipe under R_r=1, d_p=0.016 m, ε=0.9, k_s/k_f=542, F=0, Da=10^{-6}, and model A, LTNE is valid and the computed Nusselt number is Nu=6.31. Under these conditions the value of h_{sf} in the computational code was manually set to a large number of 50 to resemble LTE condition. This resulted in obtaining Nusselt number of 5.78. This value is almost identical to the Nusselt number obtained under LTE condition, Nu=5.76 [2, 3].

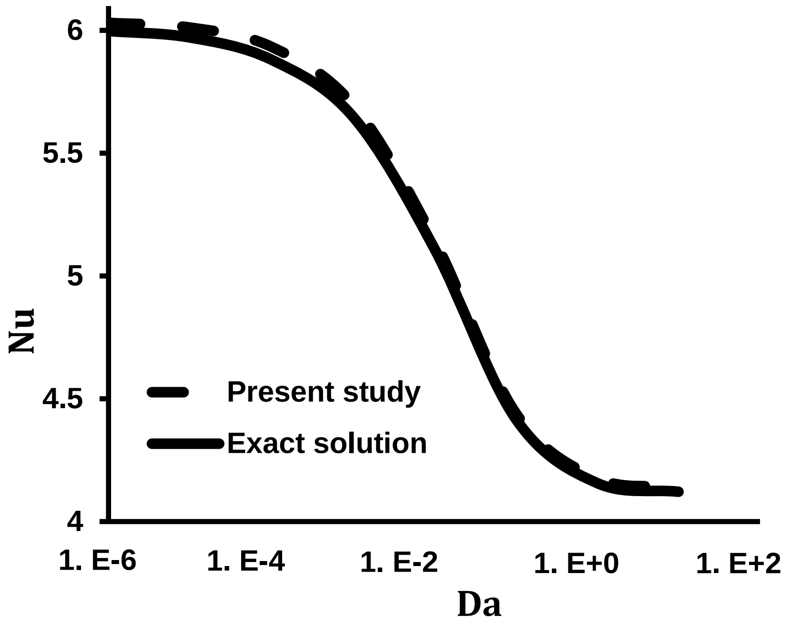

Fig. 4. Comparison of the present fully developed Nusselt number versus Darcy number for R_r = 1, k_s/k_f = 542 and LTE model, with the analytical solution of Kaviany [35].

5.1. Critical radius of the porous material for validity of local thermal equilibrium

In this section the maximum porous thickness below which the LTE condition holds, is found under model B applied at the interface. The fluid phase is air (see Table (1)) with thermal conductivity of k_f = 0.028 W.m^{-1}.K^{-1} and the solid matrix is selected to be AISA304 with thermal conductivity k_s = 15.2 W.m^{-1}.K^{-1}. This yields the conductivity ratio of k_s/k_f = 542. Figures 5 and 6 show the non-dimensional temperature of solid and fluid phases along the non-dimensional radial coordinate (Y= r/R_0). In Figs. 5a-d Darcy number is 10^{-3}. It is clear in these figures that the temperatures of the fluid and solid phases remain the same as the radius of the porous material increases up to R_r = 0.5. However, beyond this limit there is a significant disparity between the temperatures of the fluid and solid phases. These results indicate that for Darcy number of 10^{-3} the local thermal equilibrium holds up to porous thickness ratio of $R_{r,\,LTE}$ = 0.5.

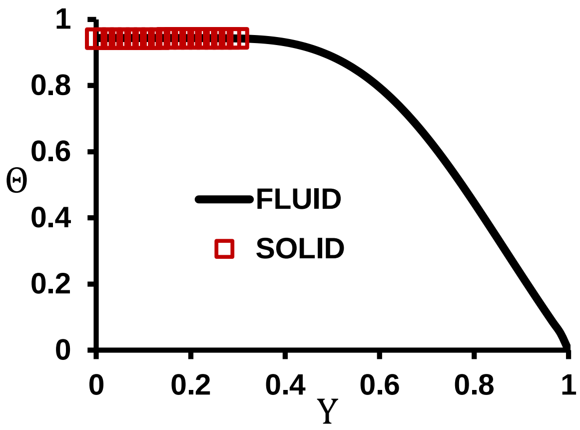

(a) $R_r = 0.3$

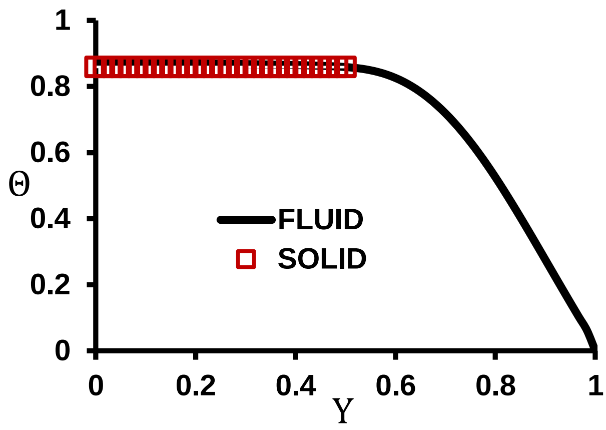

(b) $R_r = 0.5$

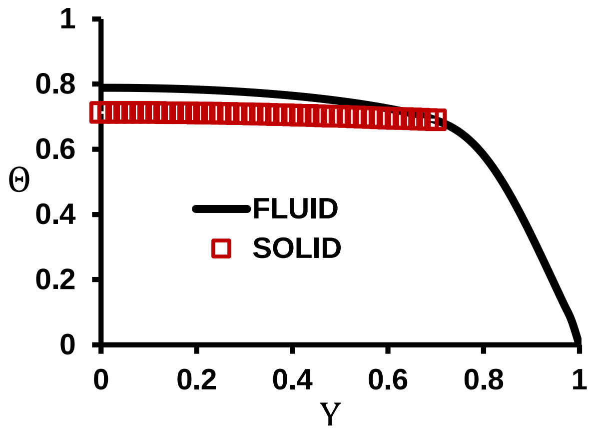

(c) $R_r = 0.7$

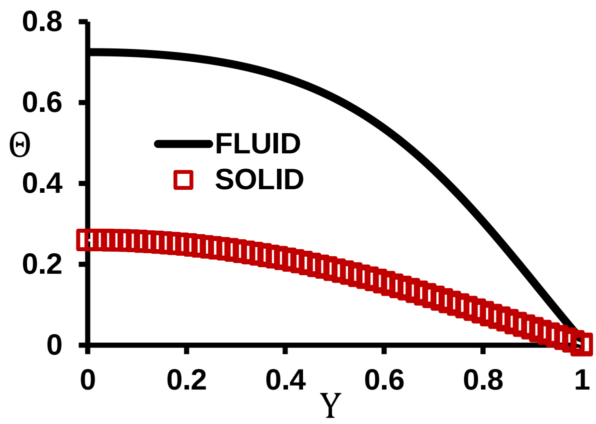

(d) $R_r = 1$

Fig. 5. Effect of porous substrate thickness on the temperature difference between the solid and fluid phases, Da = 10^{-3}, $F = 0$, $k_s/k_f = 542$, $d_p = 0.016$ m and model B.

Figures 6a-d show the non-dimensional temperature of solid and fluid phases for Darcy number of 10^{-6} and interface model of type B. It is seen in these figures that by increasing the radius of the porous material up to $R_r = 0.8$, temperature of the fluid and solid phase stay nearly the same. For the values of R_r exceeding 0.8, however, there is a temperature difference between the fluid and solid phases. Hence, for Darcy number of 10^{-6} the local thermal equilibrium holds up to $R_{r,\,LTE} = 0.8$. Although not shown here, the computations were repeated for a range of Da numbers. It was found that the maximum radius of the porous material for which the local thermal equilibrium exists ($R_{r,\,LTE}$) is inversely proportional to Darcy number. For Darcy numbers of 10^{-3}, 10^{-4}, 10^{-5} and 10^{-6} the values $R_{r,\,LTE}$ are respectively 0.5, 0.7, 0.8 and

0.8. A comparison of Figs. 5 and 6 shows that at fixed porous thickness as Da number decreases the temperature difference between the two phases increases. This behaviour can be explained by considering the hydrodynamics of the problem. It has been previously shown that for low Da numbers the fluid velocity in the porous region decreases [2, 26]. Hence, the fluid and solid phases have enough time to exchange heat and approach thermal equilibrium. Subsequently, this results in the reduction of the temperature difference between the two phases.

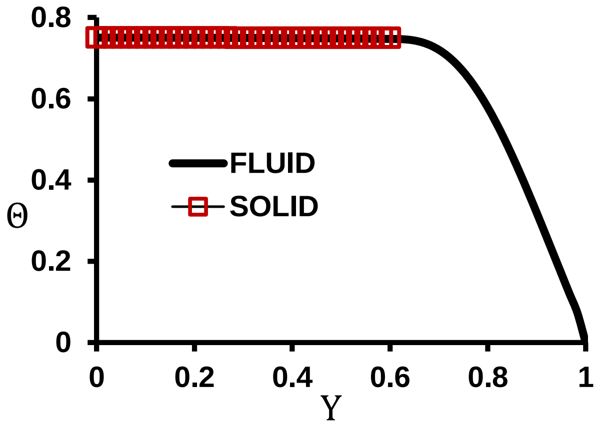

(a) R_r = 0.6

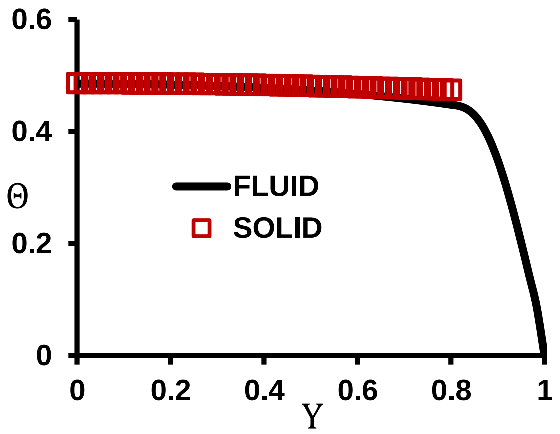

(b) R_r = 0.8

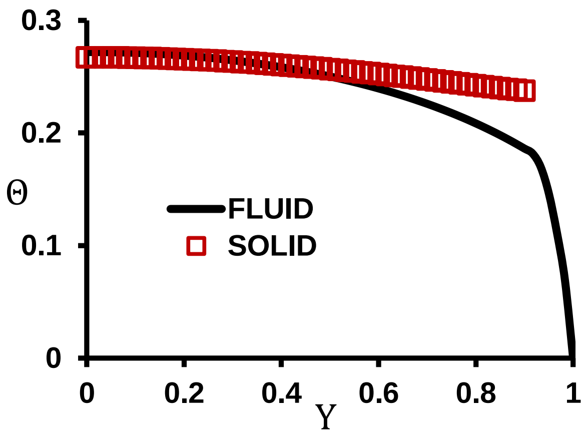

(c) R_r = 0.9

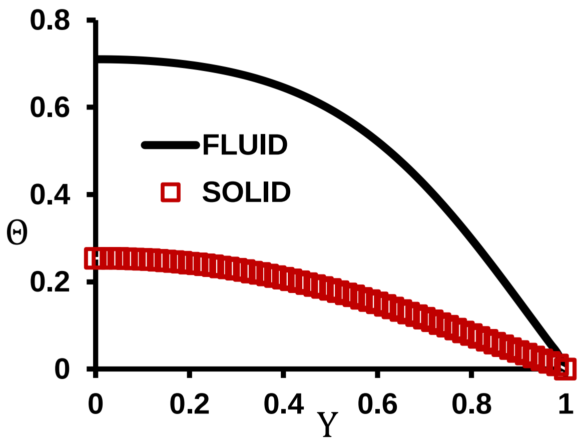

(d) R_r = 1

Fig. 6. Effect of porous substrate thickness on the temperature difference between the solid and fluid phases, Da = 10^{-6}, F = 0, k_s/k_f = 542, d_p = 0.016 m and model B.

Increasing the radius of porous material increases the convective heat transfer outside the porous media [2, 26]. Hence, a higher heat flux is delivered to the interface. Further, the conductivity ratio between the solid and fluid phases is large. Thus, the temperature difference between the two phases increases. Hence, increasing the porous thickness radius and the higher heat transfer to the porous medium are responsible for the temperature difference between the solid and fluid phases. On the other hand, through decreasing Darcy number penetration of the hot fluid into the porous medium decreases. Hence, to increase the temperature difference between the solid and fluid phases, the coefficient of convective heat transfer outside the porous media should increase. This, itself, is subjected to increasing the radius of porous material. According to Figs. 5d and 6d once the tube is fully filled with porous material the temperature difference between the two phases reaches its maximum value. It is further observed that under the fully filled condition (R_r = 1) the temperature difference between the solid and fluid phases is independent of Darcy number. Changes in the temperature difference between the solid and fluid phases are caused by the variation of fluid velocity inside the porous media. When the tube is fully filled by the porous material the fluid velocity inside the porous medium remains almost constant [2, 3, 13, 26] . Hence the rate of heat transfer between the solid and fluid phases inside the porous media is independent of Darcy number. The temperature difference between the two phases is then Darcy number independent. The present results are in keeping with the findings of the previous analytical investigations [26].

5.2. Effects of physical parameters

This section investigates the influences of various physical parameters upon the validity of LTE. These include the inertia parameter, porosity, particle diameter and conductivity ratio. It should be noted that some important physical parameters depend directly on the porosity and particle diameter. These include fluid and solid effective conductivities, permeability and consequently the Darcy number and the specific surface area. Further, the particle diameter affects the permeability, specific surface area and fluid-to-solid heat transfer coefficient. Hence, changing the porosity or particle diameter changes the specific surface area a_{sf} and the fluid-to-solid heat transfer coefficient h_{sf}. Modification of a_{sf} and h_{sf} can alter the heat transfer rate between the fluid and solid in the porous medium. This has a dominant effect on the temperature difference between the fluid and solid phases. It follows that porosity and particle diameter can have a significant effect upon the fluid and solid temperatures.

Figure 7 shows the effect of Forchheimer term on the temperature distribution in the solid and fluid phases. Computations are performed for different inertia parameter F and model B along with Darcy numbers of 10^{-2} and 10^{-6} and radius of porous material R_r of 0.8. It is observed in Fig. 7a that for a fixed Da number of 10^{-2} as the inertia increases, the general trend of temperature variations in the solid and fluid phases remains unchanged. However, the temperature difference between the two phases increases. In addition, it is seen that as the F

parameter increases the non-dimensional fluid temperature remains unchanged. However, the non-dimensional solid temperature decreases. Further, according to Fig. 7b at Darcy number of 10^{-6} increasing the inertia term has no influence upon the temperature difference between the two phases. This is due to the channelling effect that occurs in Da<10^{-3} [2, 3]. For Da = 10^{-6}, flow mainly channels between the porous medium and the pipe wall for R_r less than a critical radius [2, 3, 26]. Hence, the flow velocity inside the porous medium becomes negligible. Since most the fluid flows between the porous medium and the pipe wall, the Nusselt number should be similar to that of the corresponding annular flow. Thus for Da<10^{-3} the plug flow assumption is valid [2, 3]. It is, therefore, concluded that inertia has a significant effect on the temperature difference between the two phases at the limit of low Darcy number.

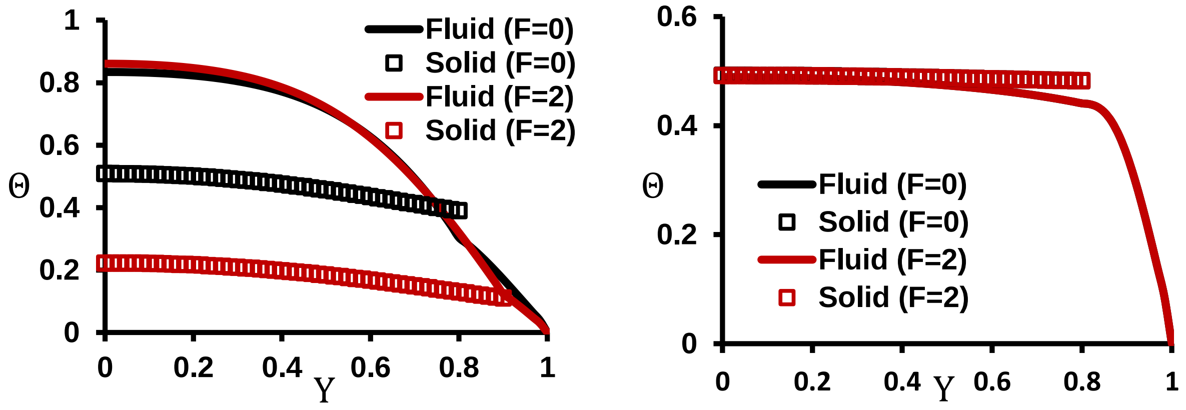

(a) Da = 10^{-2} (b) Da = 10^{-6}

Fig. 7. Effect of inertia parameter on the temperature difference between the solid and fluid phases for R_r = 0.8, k_s/k_f = 542, d_p = 0.016 m and model B.

Figure 8 shows the effect of porosity on the temperature difference between the solid and fluid phases for Da = 10^{-3} and R_r = 0.9. For low porosity (ε = 0.5) the difference between the two phases is small and LTE is valid in this limit. As the porosity increases to ε = 0.9, the fluid and solid temperatures are slightly lower than those obtained at low porosity. Nonetheless, the general trend of temperature variations is almost fixed. At high porosity the temperature difference between the two phases increases significantly and LTE is not valid anymore. When the porosity decreases, the specific surface area (see eq. (12)) increases. Hence, the heat transfer rate between the fluid and solid increases. This results in the reduction of the temperature difference between the two phases. On the other hand, as ε decrease according to eq. (10) the permeability (K) of the porous region decreases. This reduces the value of Da =

K/R_0^2. Based on the results presented in section 5.1, reduction of Da number diminishes the temperature difference between the two phases.

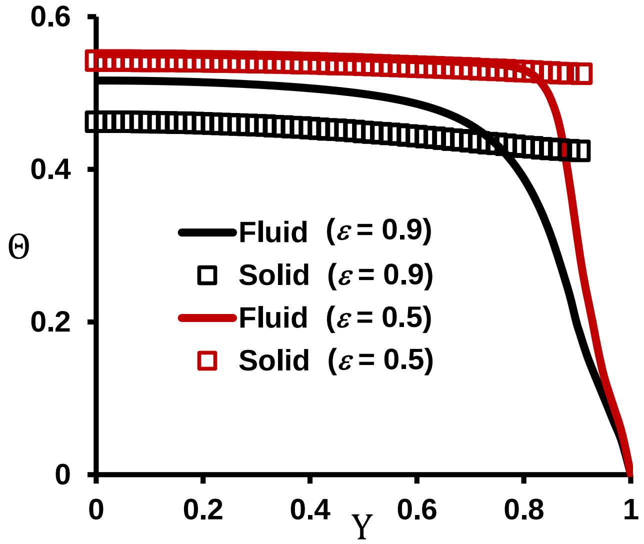

Fig. 8. Effect of porosity on the temperature difference between the solid and fluid phases, Da = 10^{-3}, R_r = 0.9, F = 0, k_s/k_f = 542, d_p = 0.016 m and model B.

Figure 9 depicts the influence of particle diameter, d_p, on the temperature difference between the fluid and solid phases for Da = 10^{-3} and porous thickness ratio of R_r = 0.9. This figure shows that as d_p increases the values of non-dimensional temperature of fluid phase increases while that of the solid phase decreases. Moreover, for low d_p the temperature difference between the fluid and solid phases is small and hence LTE is valid. As d_p increases the temperature difference between the two phases increases and LTE becomes invalid. According to eq. (13) as d_p decreases the value of fluid-to-solid heat transfer coefficient increases. Thus, the heat transfer rate between the two phases increases. This subsequently results in a low temperature difference between the two phases.

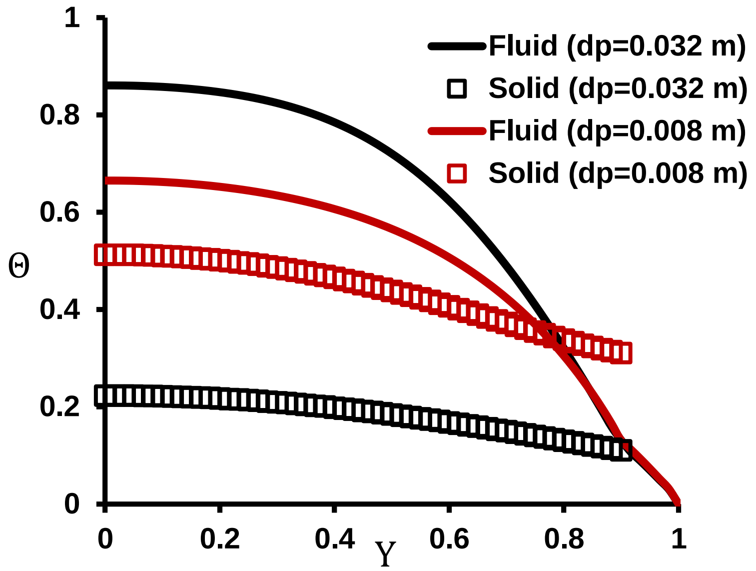

Fig. 9. Effect of particle diameter on the temperature profile for the solid and fluid phases, Da = 10^{-3}, R_r = 0.9, F = 0, k_s/k_f = 542 and model B.

Different fluid and solid materials were used in the simulation to cover a wide range of conductivity ratios (see Table (1)). Figure 10 shows the results of varying the conductivity ratio on the temperature difference between the fluid and solid phases. Conductivity ratio of $k_s/k_f \sim 2$ corresponds to the fluid phase of water and the solid matrix of soda lime and that of $k_s/k_f \sim 542$ corresponds to the fluid phase of air and the solid phase of AISI304. Figure 10 shows that for low thermal conductivity ratio, even at high Da and high porous thickness ratio, the temperature difference between the two phases is almost zero. However, as the conductivity ratio increases the difference between the solid and fluid phases increases significantly. Hence, it is concluded that for low thermal conductivity ratios the LTE condition remains valid even for a pipe with large thickness of porous material. Low ratio of solid to fluid thermal conductivity, k_s/k_f indicates that the fluid phase and solid phase have the same thermal conductivity, i.e. k_s~k_f. Further, model B states that the two phases receive the same amount of heat flux at the interface. Thus, the two phases have similar temperature and LTE holds. As the conductivity ratio increases the temperature of the solid phase becomes much higher than the temperature of the fluid phase. Therefore, according to the definition of the dimensionless temperature, the value of Θ for the solid phase becomes lower than that of the fluid phase.

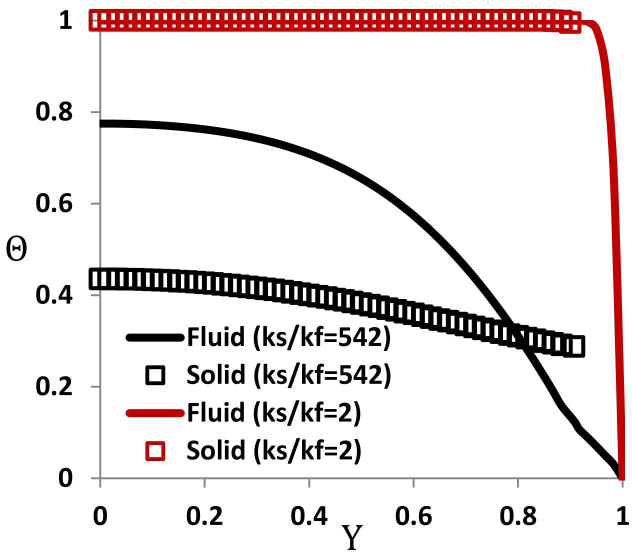

Fig. 10. Effect of conductivity ratio on the temperature difference between the solid and fluid phases, Da = 10^{-3}, R_r = 0.9, d_p = 0.016 m, F = 0 and model B.

5.3. Effects of boundary conditions on the temperature distributions

This section considers the influence of boundary conditions, models A and B (see eq. 15), on the temperature difference between the two phases at different Darcy numbers. Other parameters are set as F = 0, k_s/k_f = 542 and d_p = 0.016. The effects of Darcy number and porous thickness ratio are subsequently analysed. Figures 11, 12 and 13 show the variations in the solid and fluid temperatures for the two boundary conditions of models A and B. Darcy numbers of 10^{-3}, 10^{-5} and 10^{-6} and optimum porous material radii of 0.7, 0.8 and 0.8 corresponding to each Da number (see section 5.1) have been considered. For Da = 10^{-3} and R_r = 0.7, Fig. 11 shows that at high Darcy numbers and even for large radii of porous material the two models lead to similar results. Application of both models in this figure results in a significant temperature difference between the two phases inside the porous media. Thus, LTE does not hold anywhere inside the porous medium. Nonetheless, at the interface the temperatures of the two phases are the same and hence LTE condition holds between the two phases at the porous-fluid interface.

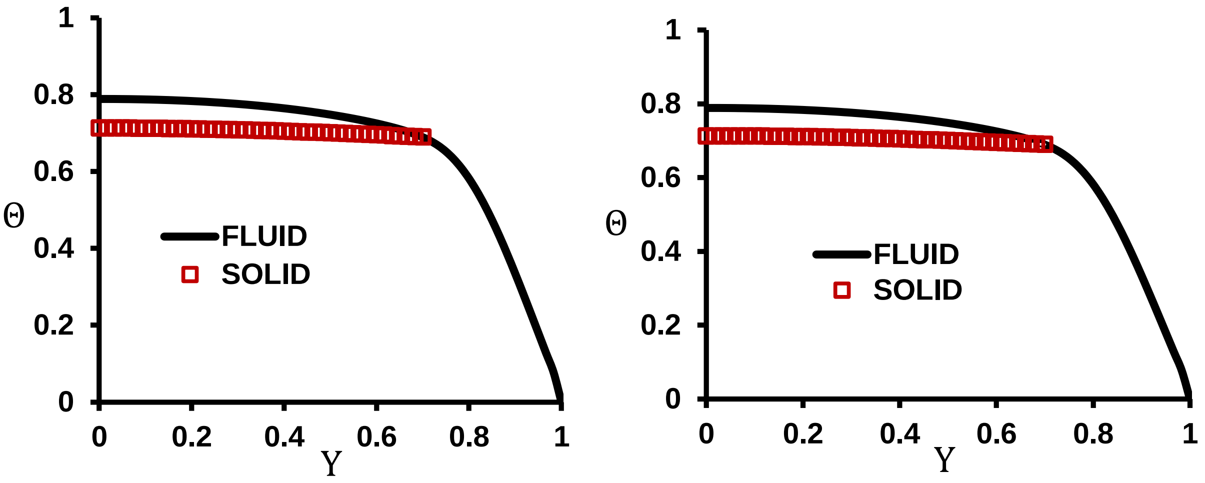

(a) Model A (b) Model B

Fig. 11. Effect of different boundary conditions on the temperature difference between the solid and fluid phases for Da = 10^{-3}, R_r = 0.7, k_s/k_f = 542 and d_p = 0.016 m and F = 0.

Figure 12 shows that as Darcy number decreases to 10^{-5} model B leads to a noticeable temperature difference between the two phases at the interface and LTE becomes invalid. However, under model A there is no temperature difference between the two phases at the interface (see eq. (15)) and LTE assumption is valid in this area. It is clear that at this value of Da number the outcomes of the two models start to diverge from each other.

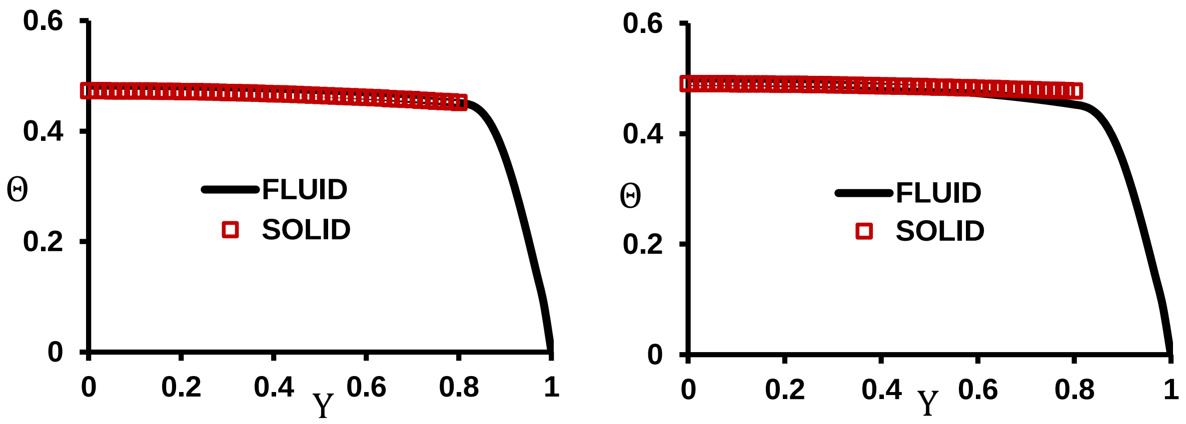

(a) Model A (b) Model B

Fig. 12. Effect of different boundary conditions on the temperature difference between the solid and fluid phases for Da = 10^{-5}, R_r = 0.8, k_s/k_f = 542 and d_p = 0.016 m and F = 0.

Further reduction of Darcy number to 10^{-6}, in Fig. 13, results in significant disparities between the outcomes of the two models at the porous-fluid interface. Model B shows no temperature difference between the two phases close to the core of the pipe. However, at the interface there exists a noticeable difference between the temperatures of the two phases and hence LTE is not valid. Conversely, model A represents LTE in the whole porous region from the core to the interface.

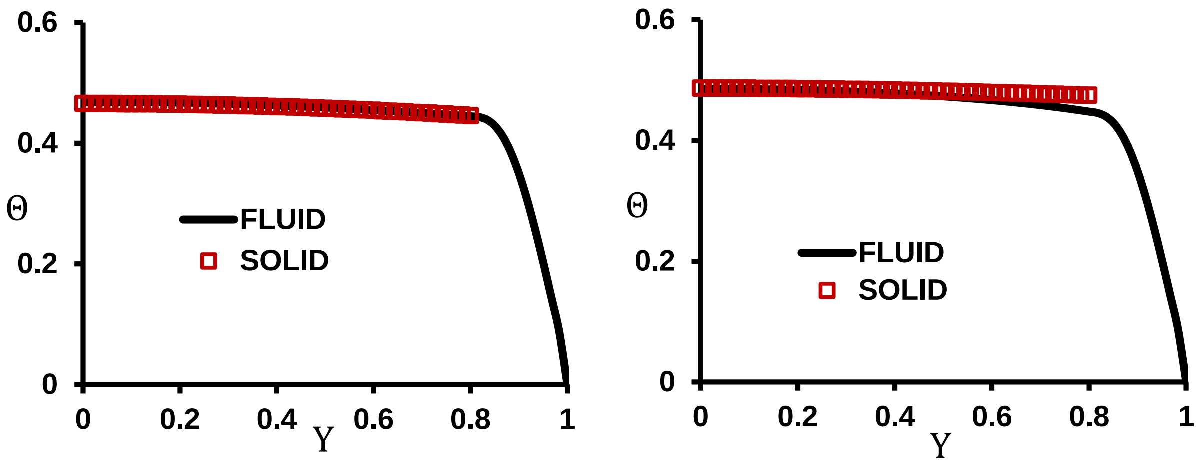

(a) Model A

(b) Model B

Fig. 13. Effect of different boundary conditions on the temperature difference between the solid and fluid phases for Da = 10^{-6} and R_r = 0.8, k_s/k_f = 542 and d_p = 0.016 m and F = 0.

Figure 14 shows the fluid and solid phase temperature distributions calculated using models A and B at low Darcy number, Da = 10^{-6}, and low porous thickness ratio of R_r = 0.6. Clearly, at this low porous thickness ratio the two models predict similar temperature distributions.

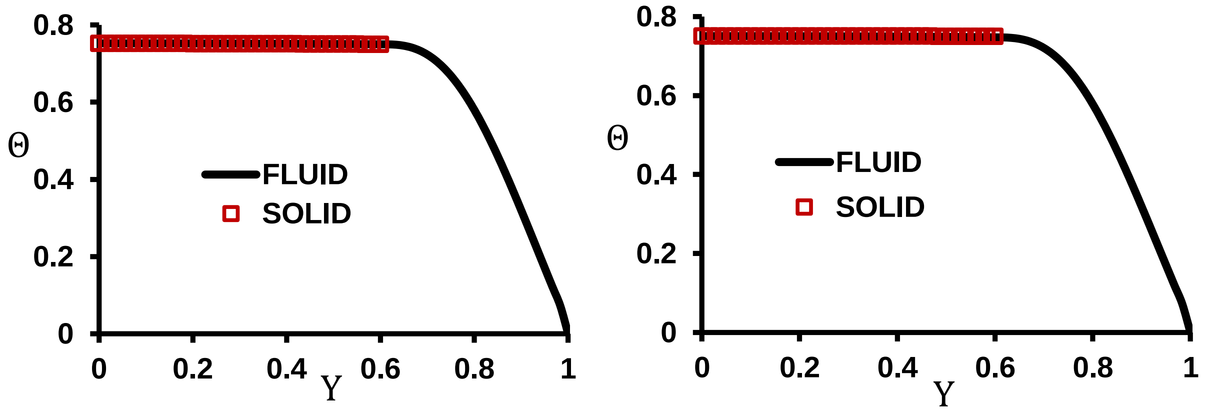

(a) Model A (b) Model B

Fig. 14. Effect of different boundary conditions on the temperature difference between the solid and fluid phases for Da = 10^{-6} and R_r = 0.6, k_s/k_f = 542 and d_p = 0.016 m and F = 0.

Simulations were repeated for other Darcy numbers. It was found that for Da of 10^{-3}, 10^{-4}, 10^{-5} and 10^{-6} the threshold porous thickness up to that the two models generate similar results are 0.8, 0.7, 0.6 and 0.6, respectively. Exceeding this threshold value results in significant disparities between the outcomes of the two models.

Determination of the proper thermal boundary condition at the porous-fluid interface is still an open question [24]. Designating one model over the other is not a trivial task as some previous studies validated both of these primary models. Further, the mechanisms of splitting the heat flux between the two phases are not fully understood yet. It is expected that various effects might cause a set of experimental results to agree with either of the two models. These effects include the variable porosity, thermal dispersion and wall thickness. In a pipe fully filled with a porous material and under constant wall heat flux, when the wall has a finite thickness made of a high conductivity material, the two phases have the same wall temperature [19]. Therefore, for this class of applications, model A is preferable. On the other hand, model B is anticipated to be a representative boundary condition for the applications with high wall temperatures and high temperature gradients. Jiang and Ren [36] showed that in a fully filled channel when the thermal conductivities of fluid and solid phases were similar, the fluid and the solid phases were close to the local thermal equilibrium. However, when the thermal conductivity between the fluid and solid phases were different they obtained good agreement between model B and the experimental data [36]. In partially filled pipe, when the heat transfer between the fluid and solid phases at the interface is large enough and their temperatures are equal at the interface, model A is applicable. However, when the heat transfer between the fluid and solid phases at the interface is not strong enough the fluid and solid temperatures at the interface are not equal and model B is preferred. Furthermore, previous works have shown that depending on the thickness of the porous material and other pertinent parameters the fluid velocity in the clear region and at the interface changes [26]. This, in turn, changes heat transfer at the porous fluid interface. Thus, depending on different parameters such as porous thickness, thermal conductivity ratio, Darcy number and inertial term either of models A or B can be applicable. For instance, at the critical porous material thickness in which the velocity gradient in the clear region is maximum, the amount of heat transfer at the porous-fluid interface is maximum and hence model A is applicable.

5.4. Nusselt number

This section investigates the dependence of Nusselt number upon the porous substrate thickness, Darcy number and inertia parameter. The aim is to further clarify the effects of the two models on the thermal behaviour of the porous flow. Figure 15 depicts the effect of porous substrate thickness on the value of the fully developed Nusselt number for different values of Da number, models A and B and two Forchheimer parameters. The Nusselt numbers are evaluated in the fully developed region at the axial location of Z = 9. It is noted that by varying Forchheimer parameters the general trend in the variation of Nu number versus R_r remains almost unchanged. In addition, the Nu number obtained for the two models are quite similar. Clearly, there is an optimum porous radius at which the Nu number is maximum. This is regarded as $R_{r,\,Nu}$. Figure 15 shows that for R_r less than $R_{r,\,Nu}$, as the porous substrate thickness increases Nu number increases. This is because increasing the porous layer thickness forces more fluid to escape to the clear region so the maximum velocity and the velocity gradient on the wall increases [2, 3, 26]. Consequently, a Nu number higher than the Nu number in a channel without porous material is achieved. However, increasing R_r to those exceeding the optimum thickness ($R_{r,\,Nu}$), reverses this trend. This is due to the fact that at large values of R_r the flow velocity and its gradient at the wall decrease [2, 3, 26]. Thus, the Nusselt number decreases. For models A and B and $F = 0$, the optimum porous thickness, $R_{r,\,Nu}$, takes the values of 0.6, 0.8 and 0.95 for Darcy numbers of 10^{-2}, 10^{-3} and 10^{-6}, respectively. However, at $F = 2$ and under both models, for Darcy numbers of 10^{-2}, 10^{-3} and 10^{-6} the values of $R_{r,\,Nu}$ are respectively 0.8, 0.8 and 0.95. Figure 15 shows that for high Darcy numbers, $R_{r,\,Nu}$ is dependent on Forchheimer parameter. Nonetheless, this is not the case at low Darcy numbers. For $Da<10^{-3}$ and R_r less than a critical radius, the flow mainly channels between the porous medium and the pipe wall [26]. Under these conditions the flow through the porous medium is negligible. Further increase in the porous thickness, to the values exceeding the optimum porous thickness, decreases the gap between the pipe walls and the porous region. This diverts the flow back into the porous region. Thus, the flow in the clear region diminishes and the Nusselt number decreases [26]. In addition, Fig. 15 shows that for high Da numbers the values of Nu number obtained through models A and B are essentially the same. However, as Da decreases the two models lead to different Nu numbers in which the Nu number obtained by model A is higher than that predicted by model B. For example, for $Da = 10^{-6}$ and $F = 2$ the Nu number based on model A is about $Nu \sim 80$ while the corresponding Nu number obtained by model B is $Nu \sim 56$.

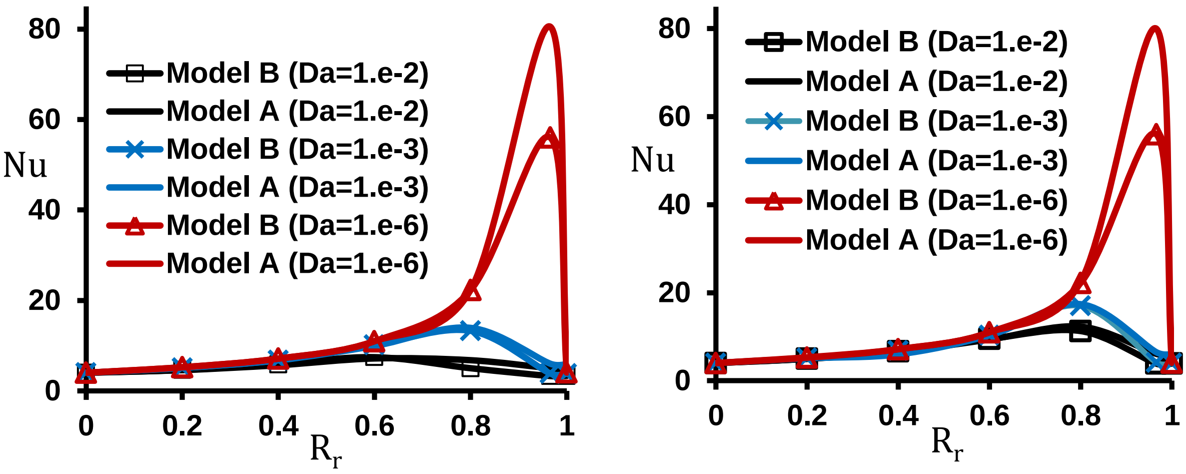

(a) $F = 0$ (b) $F = 2$

Fig. 15. Nusselt number profile for the fully developed flow versus porous thickness ratio.

In short, Fig. 15 demonstrates the followings.

1- For each value of F and for fixed Da, there is an optimum porous thickness ($R_{r,\,Nu}$) below which the two models result in similar Nu numbers. For Da = 10^{-2}, 10^{-3}, 10^{-4}, 10^{-5} and 10^{-6} the optimum porous thicknesses for $F = 0$ are 0.4, 0.75, 0.8, 0.8 and 0.8 respectively. At $F = 2$ the corresponding optimum porous thicknesses are respectively 0.7, 0.8, 0.8 and 0.8. For thicknesses greater than the critical thickness, the Nu number obtained using the two models are significantly different.

2- The Nu number determined using model A found to be considerably higher than Nu number obtained by model B. It is therefore concluded that the value of Nusselt number depends on the interface model.

3- For a given model and for Da<10^{-3}, the Nu number is independent of F. The same applies to the temperature distribution (section 5.2). However, for Da>10^{-3} as F increases the obtained Nu number increases.

4- The effects of F on Nu number for Da<10^{-3} are very similar under both models A and B. This implies that the influences of Forchheimer term on the Nusselt number under LTNE condition is independent of the thermal boundary condition at the porous-fluid interface.

5.5. Pressure loss

An important factor in heat transfer enhancement using porous materials is the pressure drop [2, 3]. The required pumping power can be inferred from the pressure loss along the duct. Figures 16a-b depict the non-dimensional pressure loss term ($-dP/dZ$) as a function of porous thickness ratio while Darcy numbers extending from 10^{-2} to 10^{-6} for (a) $F = 0$ and (b) $F = 2$.

Figure 16a shows that for F = 0 the variation of pressure drop at Da = 10^{-2} is different to the other Da numbers. However, for F = 2, Fig. 16b shows that the trend of pressure drop variation for Da = 10^{-2} is the same as the other Da numbers. In Fig. 16a for Da = 10^{-2} and F = 0, when the porous thickness increases from R_r = 0.8 to R_r = 1 the pressure drop increases smoothly. Whereas, for F = 2 as porous thickness increases a sharp increase in the pressure drop is observed. It is clear from these figures that pressure drop increases with increasing the porous thickness and reaches its maximum value when the pipe is fully filled with a porous medium, i.e. R_r = 1.

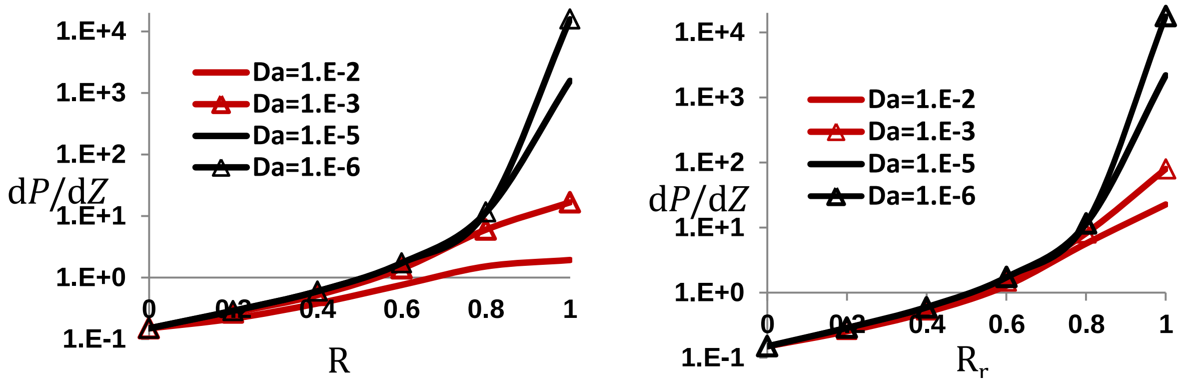

(a) F = 0 (b) F = 2

Fig. 16. Dimensionless fully developed pressure drop versus porous thickness ratio, (a) F = 0 and (b) F = 2.

Comparing Fig. 16a and Fig. 16b reveals that for Da<10^{-3} and R_r<1 the inertia parameter has no significant effect upon the pressure drop. However, for R_r = 1, as F increases the pressure drop slightly increases. For example, for Da = 10^{-5} and R_r = 1 the dimensionless pressure drop in Fig. 16a for F = 0 is ~1572 while this value in Fig. 16b for F = 2 is about 2187. On the other hand at F = 0 and F = 2 and R_r = 0.8 the pressure drop is about 11.5. It is further seen that for Da>10^{-3} the inertia parameter has a strong effect on the pressure drop. This is such that as F increases the pressure drop increases significantly. Moreover, clearly as R_r increases the effect of inertia becomes more significant and reaches its maximum at R_r = 1.

Figure 16a shows that for all Da numbers and R_r<0.4 the pressure drop is roughly independent of Darcy number. However, according to Fig. 16b for F = 2 and R_r<0.8 the pressure drop is independent of Darcy number.

In short, a close inspection of Figs. 16a and 16b reveals the followings.

- For Da<10^{-3} and R_r<1 the pressure drop is independent of the inertia parameter.
- For Da<10^{-3} and R_r<1 as the inertia parameter increases the pressure drop increases slightly.
- For F = 0 and R_r<0.4 the pressure drop is roughly independent of Darcy number.

- For F = 0, Da<10^{-3} and R_r<0.6 the pressure drop is independent of Darcy number.
- For F = 2 and R_r<0.8 the pressure drop is independent of Darcy number.

Previous works [2, 3, 5, 10, 26, 33] have shown that for R_r<0.6 the pressure drop is independent of Darcy number. The present investigation further showed that the porous thickness below which the pressure drop becomes independent of Darcy number is a function of inertia parameter. Further, for the cases of F = 0 and F = 2 and porous thickness ratio less than 0.8, Darcy number has no significant effect upon the pressure drop.

6. Conclusions

Enhancement of forced convection heat transfer in a pipe partially filled with a porous material under constant wall temperature boundary condition was studied numerically. Darcy-Brinkman- Forchheimer model was utilised to model the flow in the porous medium. Energy equations for both solid phase and fluid phase in the porous medium were solved through LTNE model. The effects of several parameters upon the flow and thermal characteristics were studied. These included the effects of porous layer thickness, Darcy number (Da), inertia parameter (F) and solid-to-fluid thermal conductivity ratio on the validity of LTE. Two models of thermal boundary conditions (models A and B) at the porous-fluid interface were applied. In model A the heat flux transferred from the external fluid to the porous material is unevenly distributed between the two phases. The distribution is on the basis of their effective thermal conductivity and the temperature gradient on the interface between the porous medium and the clear region. Model B assumes that the solid and liquid phase receive identical heat flux from the external fluid. Through application of model B, an optimum radius of porous material was determined that up to which the local thermal equilibrium (LTE) holds ($R_{r,\,LTE}$). The results show that this thickness is inversely proportional to Da number. For Darcy numbers of 10^{-3}, 10^{-4}, 10^{-5} and 10^{-6} the values of $R_{r,\,LTE}$ are respectively 0.5, 0.7, 0.8 and 0.8. It was further observed that for varying Da and different radius of the porous materials, models A and B result in different solid and fluid phase temperatures. For Da of 10^{-3}, 10^{-4}, 10^{-5} and 10^{-6} the porous thickness at which the two models generate similar results are 0.8, 0.7, 0.6 and 0.6, respectively. The influence of F at high Da was found noticeable and increasing F could lead to the reduction of temperature difference between the two phases. Further, at low Darcy numbers, F appeared to have no influence on the temperature difference between the two phases. The impacts of Da number, inertia and porous thickness on the pressure drop and Nu number for the two models A and B were then discussed. The predicted Nu number using model B found to be higher than that obtained by model B. For a given model and for Da<10^{-3}, the Nu number is independent of F. However, for Da>10^{-3} as F increases the obtained Nu number increases. It appeared that the effect of F on Nu number for Da<10^{-3} was nearly the same under both models A and B.

Acknowledgment

The authors are thankful to Dr. W. P. Breugem of Delft University of Technology for his constructive comments during the preparation of this manuscript.

Nomenclature

a	Specific surface area	m^2
C_p	Specific heat at constant pressure	J/kg. K
D_a	Darcy number	K/R_0^2
d_p	Particle diameter	m
F	Inertia parameter	
h	Fluid-to-solid heat transfer coefficient	W/m^2. K
k	Thermal conductivity	W/m. K
k_{fe}	Effective thermal conductivity of the fluid	W/m. K
k_{se}	Effective thermal conductivity of the solid	W/m. K
K	Permeability	m^2
L	Pipe length	m
Nu	Nusselt number	
p	Pressure	Pa
P	Dimensionless pressure	$p/\rho u_{in}^2$
P_r	Prandtl number	
r	Radial coordinate	m
R	Dimensionless radial coordinate	r/R_0
$R_{r,\,LTE}$	Optimum porous thickness up to which the LTE condition validates	
$R_{r,\,Nu}$	Optimum value of porous thickness which maximises the Nusselt number	
Re	Reynolds number	$\rho u_{in} R_0/\mu$
Re_p	Particle Reynolds number	$\rho u_{in} d_p/\mu$
R_p	Porous substrate thickness	m
R_0	Pipe radius	m
R_r	Ratio of porous substrate thickness to the pipe radius	R_p/R_0
T	Temperature	K
T_m	Mean temperature	K
u	Velocity in z- direction	m/s
U	Dimensionless axial velocity	u/u_{in}
U_m	Mean velocity	m/s
$\lvert u \rvert$	Velocity magnitude	$(u^2+v^2)^{1/2}$

v	Velocity in r-direction	m/s
Y	Dimensionless radial coordinate	r/R_0
z	Axial coordinate	m
Z	Dimensionless axial coordinate	z/R_0

Geek symbols

δ	Binary flag	
ε	Porosity	
Θ	Dimensionless Temperature first configuration	$\frac{T_w - T}{T_w - T_{in}}$
μ	Viscosity	kg/m. s
ρ	Density	kg/m^3

Subscripts

e	Effective
f	Fluid
in	Inlet
interface	Interface between the porous medium and the clear region
m	Bulk
p	Porous medium
s	Solid
w	Wall

References

[1] K. Vafai, Handbook of Porous Media, Marcel Dekker, Ohio, 2000, pp. 238-250.

[2] A.A. Mohamad, Heat transfer enhancement in heat exchangers fitted with porous media. Part I: constant wall temperature, Int. J. Thermal Sciences 42 (2003)385-395.

[3] M. Maerefat, S.Y. Mahmoudi , K. Mazaheri, Numerical simulation of forced convection enhancement in a pipe by porous inserts, Heat Transfer Engineering 32 (2011) 45-61.

[4] D. Poulikakos, M. Kazmierczak, Forced convection in a channel filled with porous medium, including the effect of flow inertia, variable porosity, and Brinkman friction, ASME J. Heat Transfer 109 (1987) 880-888.

[5] B.I. Pavel, A.A. Mohammad, An experimental and numerical study on heat transfer enhancement for gas heat exchangers fitted with porous media, Int. J. Heat and Mass

Transfer 47 (2004) 4939-4952.

[6] M.A. Teamah, W.M. El-Maghlany, M.M Khairat Dawood, Numerical simulation of laminar forced convection in horizontal pipe partially or completely filled with porous material, Int. J. Thermal Sciences 50 (2011) 1512-1522.

[7] V.V. Satyamurty, D. Bhargavi, Forced convection in thermally developing region of a channel partially filled with a porous material and optimal porous fraction, Int. J. Thermal Sciences 49 (2010) 319-332.

[8] K. Vafai, S.J. Kim, Analysis of surface enhancement by a porous substrate, Trans. ASME. J. Heat Transfer 112 (1990) 700–706.

[9] D. Bhargavi, V.V. Satyamurty, G.P. Raja Sekhar, Effect of porous fraction and interfacial stress jump on skin friction and heat transfer in flow through a channel partially filled with porous material, J. Porous Media 12 (2009) 1065-1082.

[10] Y.T. Yang, M.L. Hwang, Numerical simulation of turbulent fluid flow and heat transfer characteristics in heat exchangers fitted with porous media, Int. J. Heat and Mass Transfer 52 (2009) 2956–2965.

[11] E. Ucar, M. Mobedi, I. Pop, Effect of an Inserted Porous Layer Located at a Wall of a Parallel Plate Channel on Forced Convection Heat Transfer, J. Transport in Porous Media, 2013. DOI 10.1007/s11242-013-0131-4.

[12] O. Cekmer, M. Mobedi, B. Ozerdem, I. Pop, Fully Developed Forced Convection in a Parallel Plate Channel with a Centered Porous Layer, J. Transport in Porous Media 93 (2012) 179–201.

[13] K. Yang, K. Vafai, Restrictions on the validity of the thermal conditions at the porous-fluid interface: an exact solution, ASME J. Heat Transfer 133 (2011c) 112601-1-112601-12.

[14] D. Jamet, M. Chandesris, On the intrinsic nature of jump coefficients at the interface between a porous medium and a free fluid region, Int. J. Heat Mass Transfer 52 (2009) 289–300.

[15] A. d'Hueppe, M. Chandesris, D. Jamet, B. Goyeau, Boundary conditions at a fluid-porous interface for a convective heat transfer problem: analysis of the jump relations, Int. J. Heat Mass Transfer 54 (2011) 3683–3693.

[16] K. Vafai, R. Thiyagaraja, Analysis of flow and heat transfer at the interface region of a porous medium, Int. J. Heat Mass Transfer 30 (1987) 1391-1405.

[17] K. Vafai, S. Kim, Fluid Mechanics of the Interface Region Between a Porous Medium and a Fluid Layer—An Exact Solution, Int. J. Heat Fluid Flow 11 (1990) 254–256.

[18] A. Amiri, K.Vafai, T.M. Kuzay, Effects of boundary conditions on non-Darcian heat transfer through porous media and experimental comparisons, Numer. Heat Transfer, 27 Part A (1995) 651–664.

[19] D.Y. Lee, K. Vafai, Analytical characterization and conceptual assessment of solid and fluid temperature differential in porous media, Int. J. Heat Mass Transfer 42 (1999) 423-435.

[20] A. Marafie, K. Vafai, Analysis of non-Darcian effects on temperature differentials in porous media, Int. J. Heat Mass Transfer 44 (2001) 4401-4411.

[21] C. Yang, K. Ando, A. Nakayama, A Local Thermal Non-Equilibrium Analysis of Fully Developed Forced Convective Flow in a Tube Filled with a Porous Medium, J. Transport in Porous Media 89 (2011) 237–249

[22] C. Yang, A. Nakayama, W. Liu, Heat transfer performance assessment for forced convection in a tube partially filled with a porous medium, Int. J. Thermal Sciences 54 (2012) 98-108.

[23] B. Alazmi, K. Vafai, Constant wall heat flux boundary conditions in porous media under local thermal non-equilibrium conditions, Int. J. Heat Mass Transfer 45 (2002) 3071-3087.

[24] K. Vafai, K. Yang, A Note on Local Thermal Non-equilibrium in Porous Media and Heat Flux Bifurcation Phenomenon in Porous Media, J. Transport in Porous Media 96 (2013) 169–172.

[25] K. Yang, K. Vafai, Analysis of heat flux bifurcation inside porous media incorporating inertial and dispersion effects – An exact solution, Int. J. Heat and Mass Transfer 54 (2011) 5286-5297.

[26] Y. Mahmoudi, M. Maerefat, Analytical investigation of heat transfer enhancement in a channel partially filled with a porous material under local thermal non-equilibrium condition, Int. J. Thermal Sciences 50 (2011) 2386-2401.

[27] H. Dhahri, A. Boughamoura, S. Ben Nasrallah, Forced pulsating flow and heat transfer in a tube partially filled with a porous medium, J. Porous Media 9 (2006) 1-14.

[28] K. Yang, K. Vafai, Analysis of temperature gradient bifurcation in porous media – an exact solution, Int. J. Heat Mass Transfer, 53 (2013) 4316–4325.

[29] B. Alazmi, K. Vafai, Analysis of fluid flow and heat transfer interfacial conditions between a porous medium and a fluid layer, Int. J. Heat Mass Transfer 44 (2001) 1735-1749.

[30] G.S. Beavers, D.D. Joseph, Boundary Conditions at a Naturally Permeable Wall, J. Fluid Mech. 30 (1967) 197–207.

[31] F.P. Incropera, D.P. DeWitt, T.L. Bergman, A.S. Lavine, Fundamentals of Heat and Mass Transfer, Sixth ed., John Wiley & Sons, 2007.

[32] M. Peric, J.H. Ferziger, Computational Methods for Fluid Dynamics, 2nd ed., Springer, 1999.

[33] M.E. Nimvari, M. Maerefat, M.K. El-Hossaini, Numerical simulation of turbulent flow and

heat transfer in a channel partially filled with a porous media, Int. J. Thermal Sciences 60 (2012) 131-141.

[34] A. Amiri, K. Vafai, Analysis of dispersion effects and non thermal equilibrium, non-Darcian, variable porosity, in compressible flow through porous media, Int. J. Heat Mass Transfer 37 (1994) 939-954.

[35] M. Kaviany, Principle of Heat Transfer in Porous Media, second ed., Spring-Verlag, New York, 1995.

[36] P. Jiang, Z. Ren, Numerical investigation of forced convection heat transfer in porous media using a thermal non-equilibrium model, Int. J. Heat and Fluid Flow 22 (2001) 102-110.

1